

Microstructure and mechanical properties of a nanostructured Mg-8.2Gd-3.8Y-1.0Zn-0.4Zr supersaturated solid solution prepared by high pressure torsion

W.T. Sun¹, X.G. Qiao¹, M.Y. Zheng^{1*}, C. Xu², N. Gao³, M.J. Starink³

¹ School of Materials Science and Engineering, Harbin Institute of Technology, Harbin 150001, PR China

² Department of Mechanical Engineering, Nagaoka University of Technology, Nagaoka 940-2188, Japan

³ Materials Research Group, Faculty of Engineering and the Environment, University of Southampton, Southampton SO17 1BJ, UK

* zhenghe@hit.edu.cn, Tel.: +86 451 86402291, fax: +86 451 86413922

Abstract: In this study, a solution-treated Mg-8.2Gd-3.8Y-1.0Zn-0.4Zr (wt.%) alloy was processed by high pressure torsion (HPT) at room temperature, with the aim of producing a material with exceptional mechanical properties. Transmission electron microscopy and X-ray diffraction line broadening analysis reveal that a nanostructured supersaturated solid solution with a mean grain size of ~48 nm and high dislocation density of $\sim 4.7 \times 10^{14} \text{ m}^{-2}$ is achieved by HPT deformation. After HPT processing, the present solution-treated samples show finer grains and higher dislocation densities as compared to as-cast samples of this alloy, other solution-treated Mg-RE alloys and conventional Mg alloys deformed using similar HPT processing conditions. This could be attributed to retardation of the dislocation annihilation through enhanced solute-dislocation and / or dislocation-dislocation interactions. The higher dislocation density and nanosized grains within supersaturated solid solution cause the microhardness to increase to ~126 HV, which is higher than that of the as-cast Mg-8.2Gd-3.8Y-1.0Zn-0.4Zr (wt.%) alloy processed by HPT, and is also higher than that of any conventional Mg-rich alloy deformed using HPT.

1. Introduction

Magnesium alloys are well-known light structural materials that are applied in automobile and aircraft industries because of their low density and high specific strength and stiffness [1, 2]. Recently, alloying Mg with rare earth (RE) elements has attracted tremendous attention due to the improved strength at both room and elevated temperatures [3, 4]. In Mg-RE castings the coarse matrix grains and eutectic network-shaped second phases formed during solidification degrade the strength and ductility of castings. Thermo-mechanical processing, such as extrusion and rolling [5, 6], is often used to refine the microstructure of Mg alloys. However, with these conventional processing methods it is difficult to obtain a sufficiently refined microstructure for strengthening owing to the limited strain imposed. Additionally, it needs to be considered that thermo-mechanical processing of these alloys is difficult due to number

of factors. One factor is that the hexagonal close-packed (hcp) crystal structure has limited independent slip systems, and hence conventional thermo-mechanical processing at low temperatures can lead to cracking. Therefore, deformation processing should be performed at relative high temperature to activate non-basal plane slip. However, high temperature processing will generally limit the grain refinement during processing.

To investigate a possible alternative way of improving the microstructure of Mg-RE alloys by thermo-mechanical processing, in this work high pressure torsion (HPT) is applied. HPT processing, as a kind of severe plastic deformation (SPD) technique, offers the possibility of significant grain refinement even down to nanometer scale by introducing intense strains without changing the geometry of samples [7]. As compared to other SPD procedures, application of quasi-hydrostatic pressure in HPT prevents cracking, so HPT can be used to deform Mg alloys at low temperature to produce bulk ultrafine-grained Mg alloys [7]. However, limited work on HPT processing of Mg-RE alloys has been conducted, with works to date primarily focusing on binary Mg-Gd [8], Mg-Dy-Al-Zn-Zr [9] and Mg-Gd-Y-Zr [10, 11] alloys. In these works, the hardness of the HPT-processed Mg-RE alloys studied was generally lower than 110 HV over all or most of the disk, i.e. a fairly modest hardening as compared to conventionally processed commercial Mg alloys was achieved. For example, HPT processing at room temperature (RT) for 5 turns of as-homogenized Mg-10Gd (wt.%) alloy caused a grain size refinement to about 100 nm and a microhardness of 105 HV was obtained [8]. Radim et al. reported that when only 3 turns of HPT processing was performed on solution-treated Mg-9.4Dy-2.0Al-0.7Zn-0.2Zr (wt.%) alloy at RT, the average microhardness was increased nearly to 95 HV [9], but they did not evaluate the influence of different strain levels (i.e. by increasing the number of revolutions) on microstructure and microhardness evolutions. In other work, an as-extruded and subsequently homogenized Mg-8Gd-3Y-0.4Zr (wt.%) alloy was subjected to 5 turns of HPT processing at RT and the microhardness varied from 90 HV at the centre to 125 HV at the periphery, which was ascribed to the successive grain subdivision through deformation twinning [10]. The formation of partially nanocrystalline structure with non-uniformed grain sizes of 20-90 nm upon HPT of as-extruded Mg-4.7Y-4.6Gd-0.3Zr (wt.%) alloy after 10 turns at RT resulted in substantial hardening by up to ~40 HV relative to the undeformed state of the alloy [11].

It is known that Gd and Y have very high solubility in α -Mg, leading to significant solid solution strengthening efficiency [12-14] and hence a Mg-8.2Gd-3.8Y-1.0Zn-0.4Zr (wt.%) alloy, with high Gd and Y alloy is investigated. In our previous work, the Mg-8.2Gd-3.8Y-1.0Zn-0.4Zr (wt.%) alloy was subjected to HPT processing at RT starting from an as-cast condition. This caused the average grain size to decrease from

~85 μm to ~55 nm as the equivalent strain increased to ~6.0, and the corresponding microhardness reached a saturated value of about 115 HV [15]. As research on the influence of initial solid solubility, particularly the effect of high content of dissolved RE elements, on evolution of microstructure and hardness of Mg-Gd-Y alloys during HPT has so far been limited, we have performed a detailed study on the effect of HPT on solution-treated Mg-8.2Gd-3.8Y-1.0Zn-0.4Zr (wt.%). We particularly aim to investigate whether through SPD it is possible to obtain a Mg-rich alloy with homogeneous high hardness (well above 120 HV) combined with a homogeneously refined microstructure that should provide good ductility. The variations of microstructure and hardness with the imposed HPT strain were examined. This work is expected to deepen the understanding of the formation of nanostructured Mg-RE supersaturated solid solutions during HPT.

2. Experimental procedures

A high quality Mg-8.2Gd-3.8Y-1Zn-0.4Zr (wt.%) ingot with 280 mm in diameter and 2940 mm in length was fabricated by direct-chill casting using pure Mg (>99.99%) and Zn, Mg-30Gd (wt.%), Mg-30Y (wt.%) and Mg-25Zr (wt.%) master alloys. In order to guarantee the same composition of each initial sample for HPT processing, the billet was cut from one half the radius of the as-cast ingot. Subsequently, the solid solution treatment was performed at 510 °C for 12 h, followed by an immediate warm water quench at 60 °C [16, 17]. The solutionized billet was cut into disks with a diameter of 10.0 mm and a thickness of 1.0 mm. These disks were ground with abrasive papers on both sides to final thicknesses of ~0.85 mm with parallel broad surfaces, and then processed by HPT for 1/8, 1, 2, 5, 10 and 16 turns at ambient temperature under quasi-constrained conditions [7] with an imposed pressure of 6.0 GPa and a rotational speed of 1 rpm.

The microstructures of the specimens were examined by optical microscopy (OM), an FEI field-emission scanning electron microscope (FE-SEM) with energy dispersive spectrometer (EDS), and an FEI-TECNAI G2 transmission electron microscope (TEM) operating at 300 kV. For TEM observation, thin disks with a diameter of 3.0 mm were punched from the HPT samples, with the centre of the TEM disk located at a position 2.5 mm from the centre of the HPT disk. These punched disks were mechanically polished to ~50 μm in thickness and subsequently ion-milled by a Gatan plasma ion polisher. The average grain sizes of HPT-processed samples were determined from TEM images using the modified line intercept method [18], and the grain size D was taken as $D=1.455\bar{L}$, where \bar{L} is the average line intercept [19, 20]. Analysis of the constituent phases and texture of as-cast, solution-treated and HPT-processed samples were carried out using an X'Pert PRO X-Ray diffractometer (XRD).

For each disk of different HPT turns, 3 runs of XRD analysis was carried out to reduce errors and improve accuracy. The dislocation densities ρ of the samples were deduced from the measured microstrains $\langle \varepsilon^2 \rangle^{1/2}$ and crystallite sizes D_c , which are determined by analyzing the XRD line profiles via the Materials Analysis Using Diffraction (MAUD) software [21, 22]. Details of this dislocation density determination method were described previously in Ref. [20]. The method uses the following equation [20, 23, 24] to determine the dislocation density, ρ :

$$\rho = \frac{2\sqrt{3}\langle \varepsilon^2 \rangle^{1/2}}{D_c b} \quad (1),$$

where b is the Burgers vector.

The variation of solid solubility of solute atoms with temperature under 1 atm was calculated using PandatTM 2017 (Compu Therm LLC) with the latest PanMg database [25].

The distributions of Vickers microhardness along the diameters of each disk were measured with incremental steps of 0.5 mm using a Zwick microhardness tester under a constant load of 500 gf held for 15 s. Prior to hardness measurement, each disk was carefully ground with SiC abrasive papers of 800, 2000 and 4000 grit and then polished to a flat mirror-like surface by using a cloth with colloidal silica suspension and 1 μ m diamond paste. Each reported hardness was taken as the average value of four separate indentions at positions with a same distance to the centre of the disk. The dependence of Vickers microhardness on the equivalent strain of HPT-processed Mg-Gd-Y-Zn-Zr disks was also investigated. The equivalent strain imposed on the disk has been given as [26, 27]:

$$\varepsilon_{eq} = \frac{2}{\sqrt{3}} \ln \left[\left(1 + \frac{\gamma^2}{4} \right)^{1/2} + \frac{\gamma}{2} \right] \quad (2)$$

$$\gamma = \frac{2\pi r N}{h} \quad (3),$$

where γ represents the shear strain, r is the radial distance from disk centre, h is the thickness of the disk and N is the total number of torsional revolutions.

3. Results

3.1 Microstructure evolution during HPT processing

Fig. 1 shows OM and TEM micrographs that reveal the microstructure of the Mg-8.2Gd-3.8Y-1Zn-0.4Zr (wt.%) alloy before and after solid solution treatment. The as-cast material shows a substantial amount of second phase particles on a network at the grain boundaries (Fig. 1(a)), but after solution treatment most of the second phases at the grain boundaries are dissolved (Fig 1(b)), and a supersaturated Mg-Gd-Y-Zn-Zr solid solution is obtained. Solution treatment causes the grain size to increase to about 90 μ m as seen in Fig 1(b) and in addition to a few discontinuous equilibrium β phase

(Mg₅RE, fcc structure, $F\bar{4}3m$, $a=2.23$ nm [17, 28]) particles at the grain boundaries, a small amount of lamellar-shaped particles are formed near the Mg₅RE phase (Fig 1(c)). Through HRTEM analysis these lamellar particles are identified as 14H long-period stacking ordered (LPSO) phase (Fig 1 (d)).

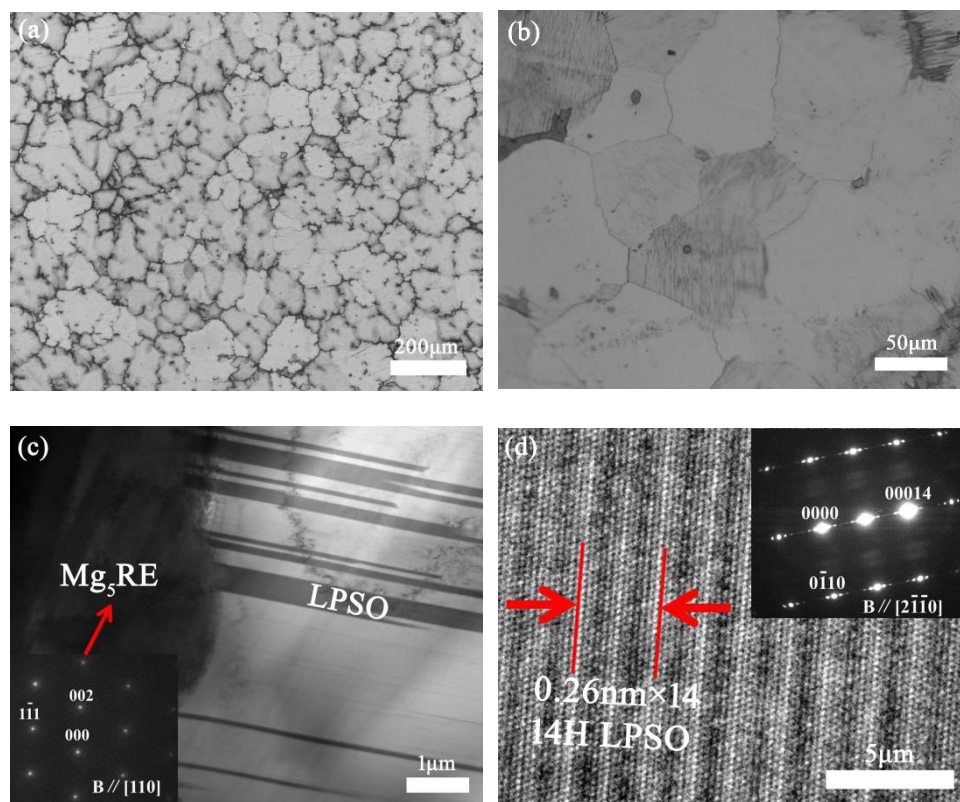


Fig.1 Optical microstructure of the (a) as-cast and (b) solution-treated Mg-Gd-Y-Zn-Zr alloy; (c) TEM micrograph of Mg₅Gd and LPSO phase in the solutionized alloy; (d) HRTEM image and inserted SAED pattern of LPSO phase shown in (c).

Fig.2 shows OM micrographs revealing the evolution of microstructures at different regions (centre, 1/2 radius and edge) of the disks after HPT for various revolutions. It can be seen that after 5 turns the grain refinement at the edge has progressed such that grain boundaries at the edge region could no longer be resolved by OM. In contrast to this, the microstructure in the central area develops much more slowly, and this is due to the decrease of strain from the edge to centre of disk during HPT processing [7, 29, 30]. The evolution in microstructure at half radius is similar to that at the periphery, but more revolutions are needed to achieve dramatic grain refinement. Furthermore, there is almost no difference detectable in microstructure between HPT10 and HPT16.

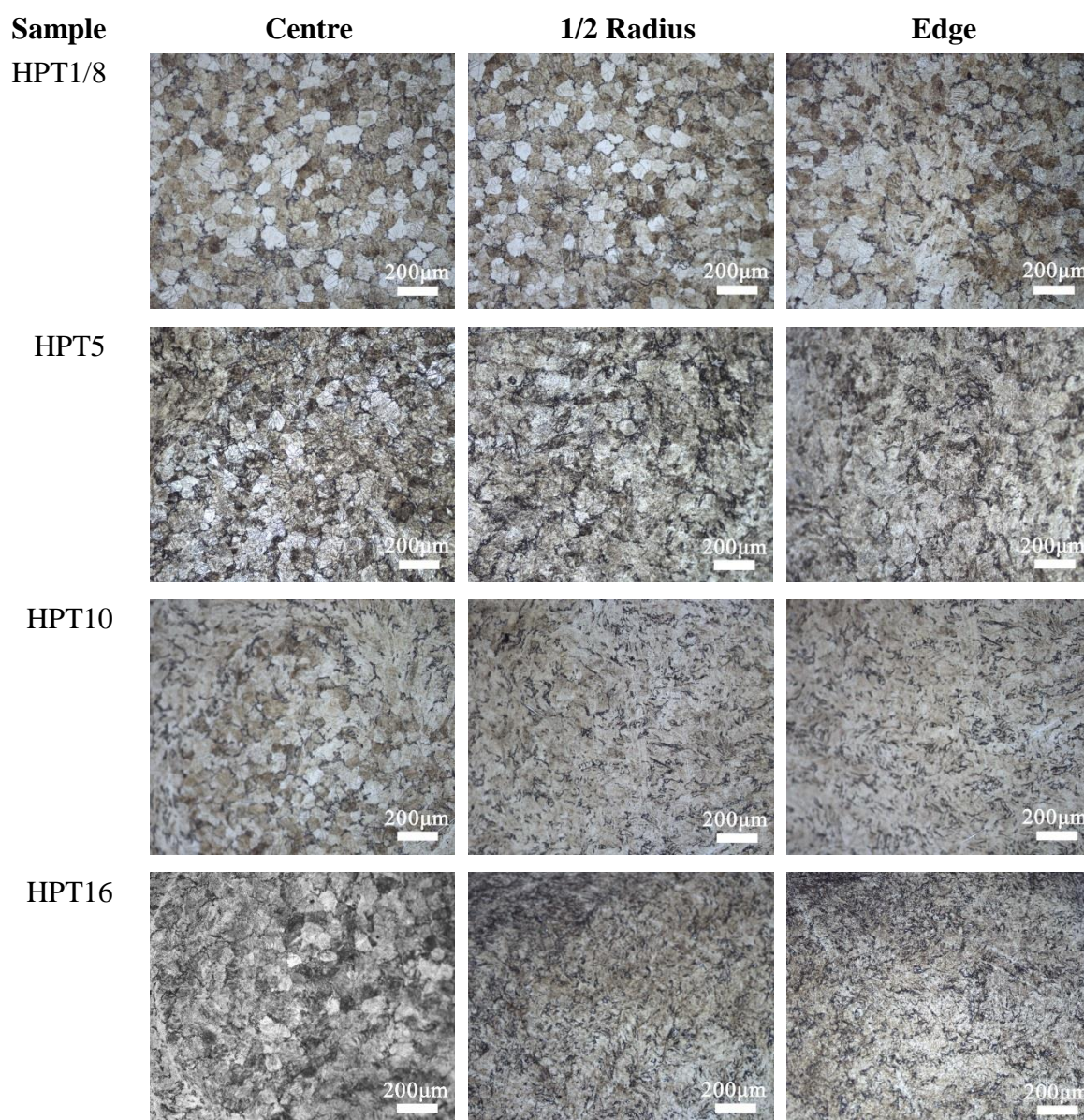


Fig.2 Optical micrographs of solutionized Mg-Gd-Y-Zn-Zr disks processed by HPT for various revolutions taken at positions close to the centre (left column), 1/2 radius (central column) and periphery (right column).

To illustrate the evolution of grain refinement during HPT processing, TEM images and corresponding SAED patterns of HPT-processed samples with different revolutions are shown in Fig. 3. At the beginning of deformation, after 1/8 turn, the areas of high density of dislocation pile-ups and tangles are visible in the matrix, as shown in Fig. 3(a). After 5 turns (see Fig. 3(b)) many dislocation cells are generated, which is reflected by the arcs of diffraction spots in the corresponding SAED patterns. In Fig. 3(c) and (d), both bright field and dark field TEM images demonstrate that HPT for 10 turns produces homogeneous fine grains with a mean size of 48 ± 4 nm, and the

corresponding SAED patterns exhibit diffraction rings, which indicates that the sample contains nanoscaled grains with high-angle grain boundaries. It is apparent that the grain size of Mg-Gd-Y-Zn-Zr decreases with increasing HPT revolutions, and reaches a saturated state after about 10 turns. No additional diffraction spots apart from Mg matrix rings are detected in the SAED patterns after HPT 16 turns, suggesting that no new precipitate phase is formed. This indicates a supersaturated solid solution of nanosized Mg-rich α phase grains is obtained.

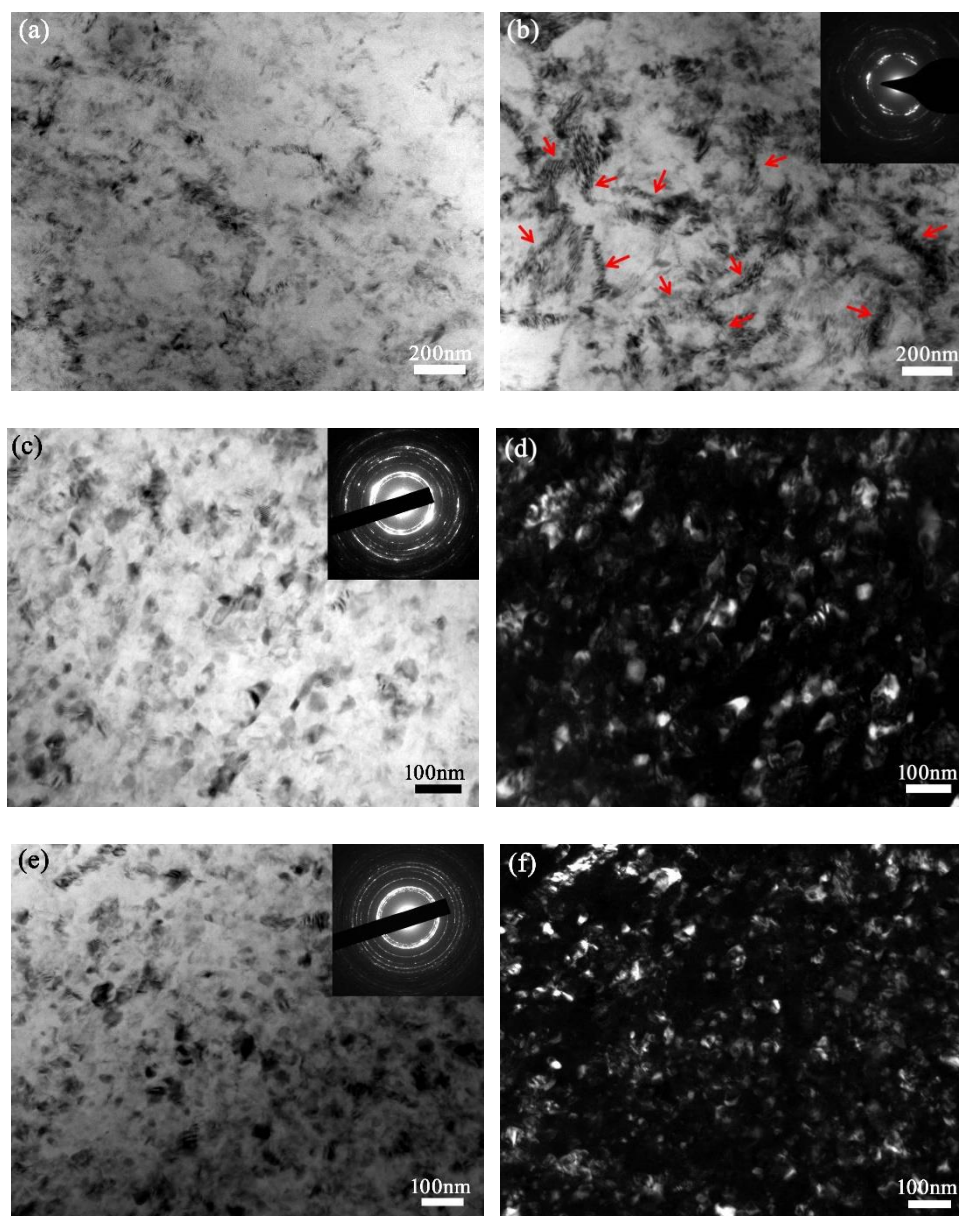


Fig.3 TEM bright field images and corresponding SAED patterns taken from the positions close to 1/2 radius of Mg-Gd-Y-Zn-Zr disks processed by HPT for various revolutions: (a) HPT1/8; (b) HPT5; (c) HPT10; (d) dark field image of (c); (e) HPT16; (f) dark field image of (e).

EDS analysis by SEM of the Mg-rich matrix of the sample processed by 10 turns of HPT reveals a composition of 7.86 ± 0.02 wt.% Gd, 3.72 ± 0.05 wt.% Y, and 0.65 ± 0.03 wt.% Zn. These contents of solutes in the α -Mg matrix are slightly increased in comparison with that of the initial solutionized sample, which has a composition similar to the equilibrium solubility of solutes at 510 °C obtained by phase diagram calculation (see Fig. 4(a) and (b)). Moreover, it is noted that for such a saturated state achieved by HPT, the contents of solutes in the matrix substantially exceeds the calculated theoretical values of equilibrium solubility limit in Mg matrix at the HPT-processing temperature of 25 °C as shown in Fig. 4(c). For comparison the Mg matrix of an as-cast alloy followed by HPT processing of 10 turns is also analyzed and this reveals 4.72 ± 0.08 wt.% Gd, 2.70 ± 0.02 wt.% Y, and 0.33 ± 0.07 wt.% Zn.

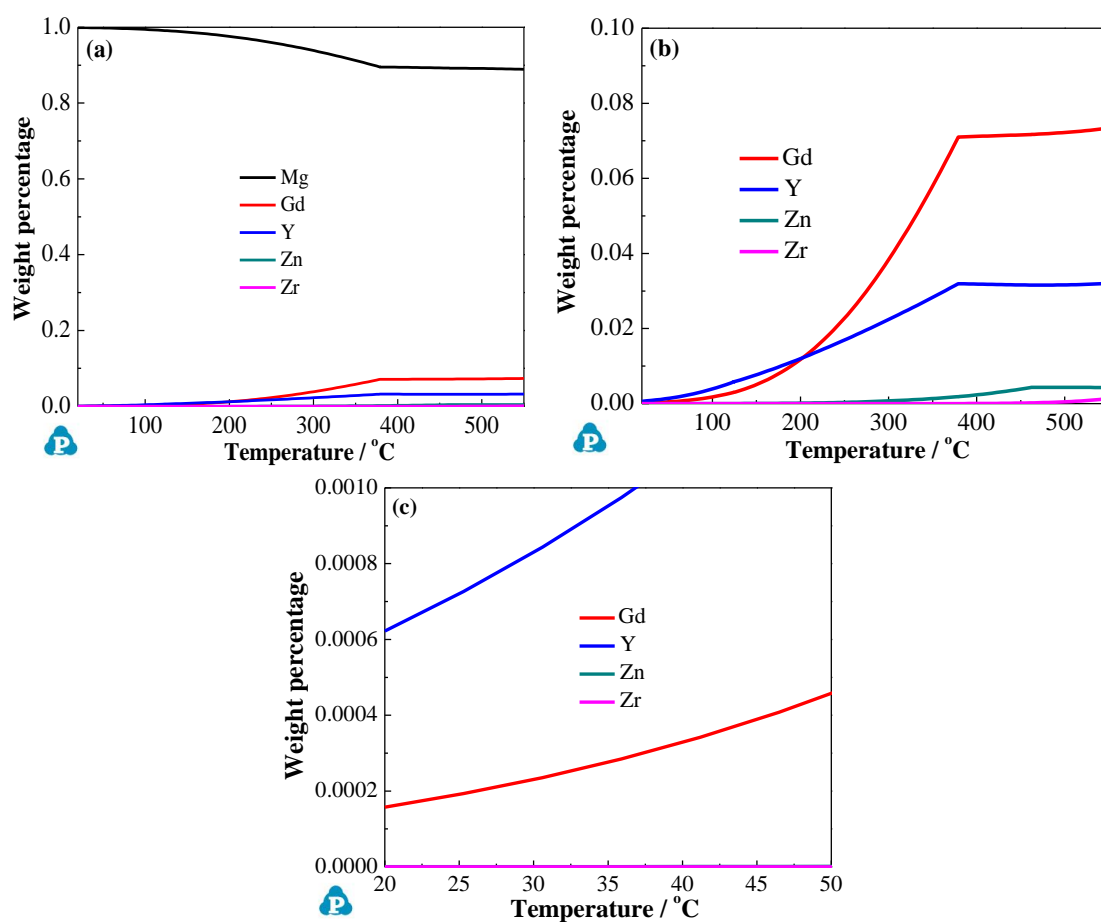


Fig.4 (a) Variation of solid solubility of solutes with temperature under 1 atm; (b) enlarged section in the range from 0 to 0.1 wt.%; (c) enlarged section in the range from 20 °C to 50 °C.

3.2 XRD analysis

The XRD patterns of the initial Mg-Gd-Y-Zn-Zr alloy after solution heat treatment and HPT processing with different revolutions are shown in Fig. 5. The XRD data do not show any peaks due to a second phase, indicating that the fraction of second phase is below the detection threshold of XRD measurement (typically ~5 vol.%). In comparison with the solutionized sample, the positions of XRD peaks from the α -Mg phase in the HPT-processed samples are shifted to slightly lower angles (see Fig. 5(b)). This suggests that the residual second phases (see Fig 1(c)) are dissolved into the matrix with increasing imposed strain. Similarly, our previous research also demonstrated that HPT caused some fragments of second phase to partially dissolve into the Mg-rich matrix phase [15].

The variations of both lattice axial ratio c/a and dislocation density with HPT revolutions obtained from XRD data are shown in Fig.6. The lattice axial ratio c/a of the hcp crystal structure can be used to evaluate the degree of lattice distortion which is related to the composition of the Mg-rich phase [31]. Both experimental data and first-principles calculations [32-34] have indicated that c/a reduces with the increasing RE solutes dissolved in the Mg-rich phase. In our solution-treated sample, the c/a of the Mg solid solution deviates only slightly from that of pure Mg (1.6236) [31, 33] and with increasing HPT turns, c/a decreases significantly to reach 1.612 after 16 turns (see Fig.6, blue squares), suggesting that the content of solute atoms in the α -Mg matrix increases due to dissolution of residual second phases.

The dislocation density as measured by line broadening analysis increases to $\sim 4.7 \times 10^{14} \text{ m}^{-2}$ after 10 turns and remains almost unchanged on further deformation (see Fig.6, red triangles), thus indicating the deformation-induced microstructure evolution has saturated.

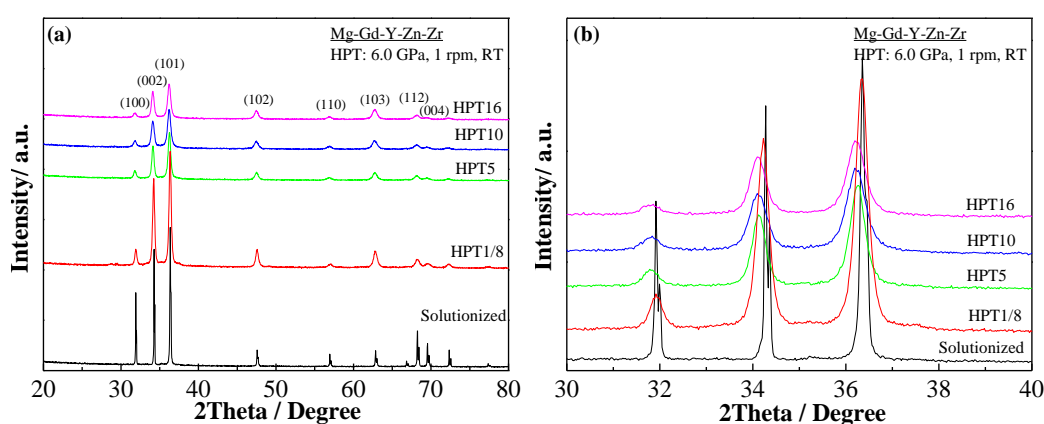


Fig.5 (a) XRD patterns of the solutionized and HPT-processed Mg-Gd-Y-Zn-Zr alloy with various revolutions; (b) enlarged section of the XRD patterns.

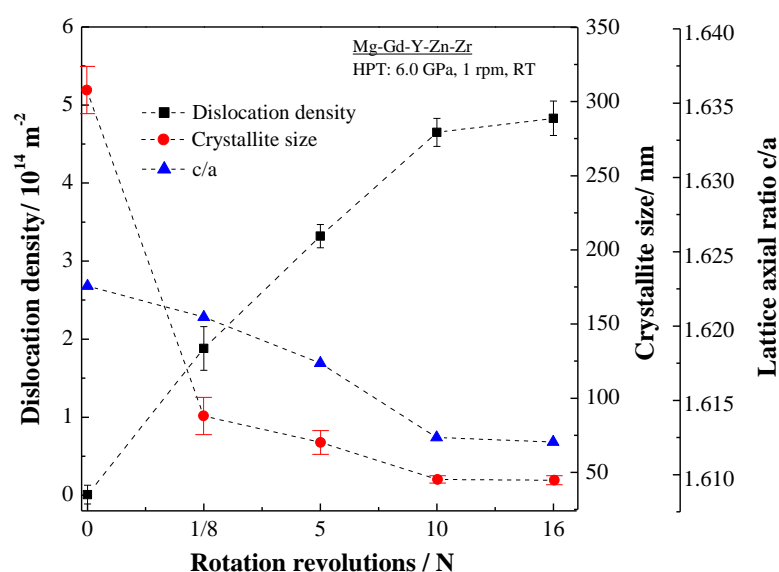


Fig. 6 Dislocation density, crystallite size and lattice axial ratio c/a of the solutionized and HPT-processed Mg-Gd-Y-Zn-Zr alloy as a function of the number of HPT revolutions.

3.3 Texture evolution

Fig.7 shows the (0002) pole figures of the as-solutionized and HPT-processed Mg-Gd-Y-Zn-Zr alloys. The as-solutionized sample (i.e. prior to HPT) exhibits nearly random grain orientation distributions, as shown in Fig. 7(a), whereas after HPT a strong basal texture with basal (0002) planes perpendicular to compressive direction is formed, as seen Fig. 7(b) to (e). The development of this texture can be explained by the fact that the critical resolved shear stress (CRSS) required for basal slip at ambient temperature is less than that for non-basal slip systems, leading to an easy activation of basal slip plane of grains towards the preferred orientation, and the c -axis is constrained parallel to compression direction. Basal texture has been observed in a range of other Mg alloys after HPT processing, such as Mg-Gd [8], Mg-Dy-Al-Zn-Zr [9] and ZK60 [35].

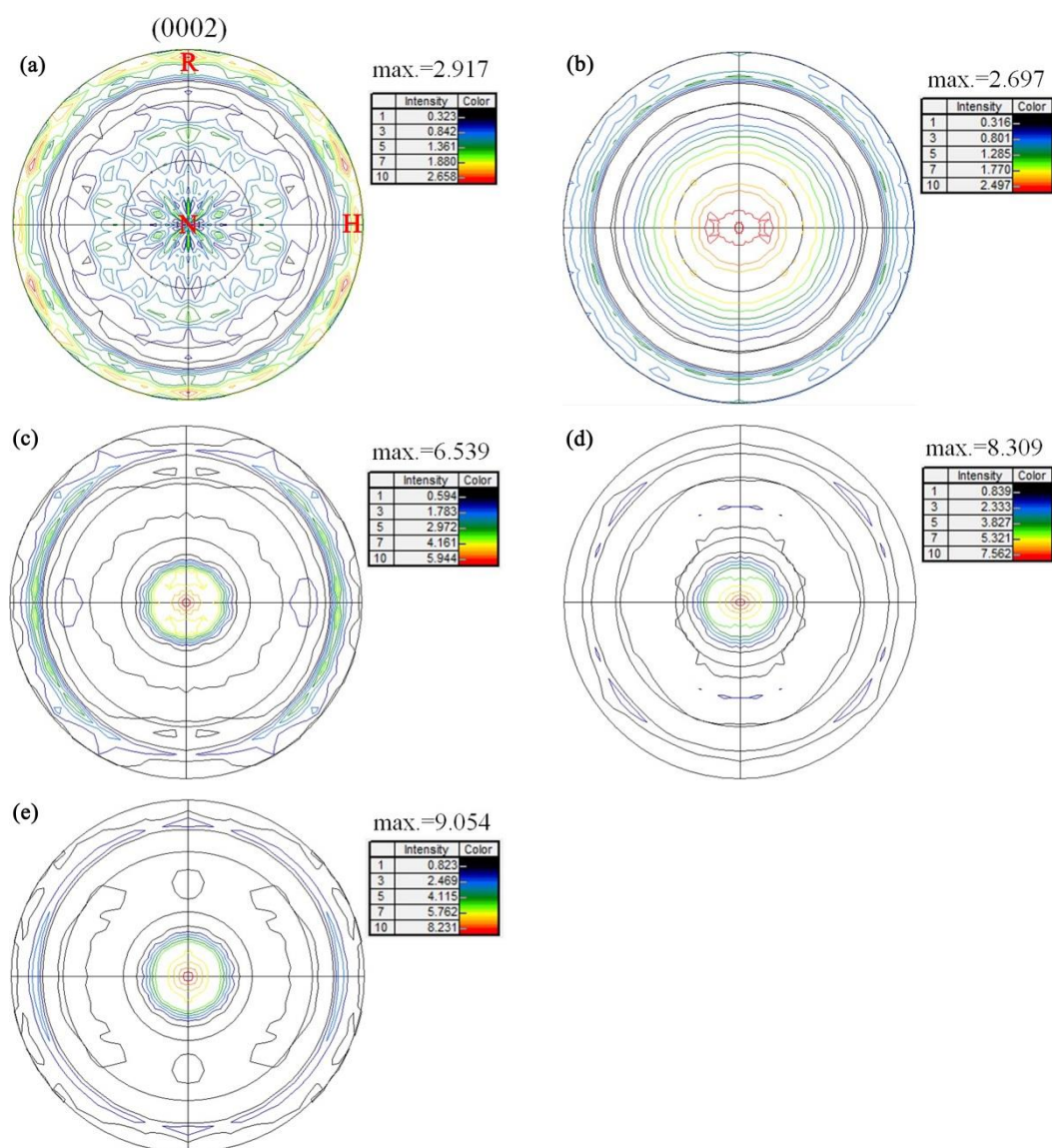


Fig.7 (0002) Pole figures of solutionized and HPT-processed Mg-Gd-Y-Zn-Zr alloy with various revolutions: (a) solutionized; (b) HPT1/8; (c) HPT5; (d) HPT10 and (e) HPT16. R and N represent radial, and compression direction, respectively.

3.4 Microhardness evolution

The dependence of microhardness on the number of revolutions and the equivalent strain imposed by HPT are plotted in Fig. 8(a) and (b), respectively. As shown in Fig. 8(a), the microhardness of the Mg-Gd-Y-Zn-Zr alloy after solid solution heat treatment (i.e. prior to HPT processing) is approximately 93 HV and the microhardness increases significantly due to HPT processing. With increasing HPT turns, the scattering of microhardness along the diameter is decreased and also the difference in hardness between the centre and the periphery region decreases. As shown in Fig. 8(b), strain hardening takes place for equivalent strain up to ~6.0, and with further increase of strain

the microhardness remains almost constant at 126 ± 2 HV. The microhardness evolution of as-cast Mg-Gd-Y-Zn-Zr alloy directly deformed by HPT under the same conditions was determined in a previous study [15], and this data is also plotted in Fig. 8(c). By comparison, solid solution treatment prior to HPT deformation causes a higher hardness after 16 turns. The variation of microhardness with equivalent strain in double log coordinates, as plotted in Fig. 8(d), shows a linear relationship. The solid straight line for HPT-deformed Mg-Gd-Y-Zn-Zr solution-treated alloy gives the relationship for the hardness $HV \approx 107HV_{\epsilon_{eq}}^{0.09}$, where the unit of hardness is HV, i.e. the hardening exponent [35, 36] determined by the slope is ~ 0.09 . The data the as-cast alloy processed by HPT also shows a linear relationship in the double log plot, but the slope is lower with a hardening exponent of ~ 0.05 . This indicates that strain hardening rate is dependent on the initial state prior to HPT processing.

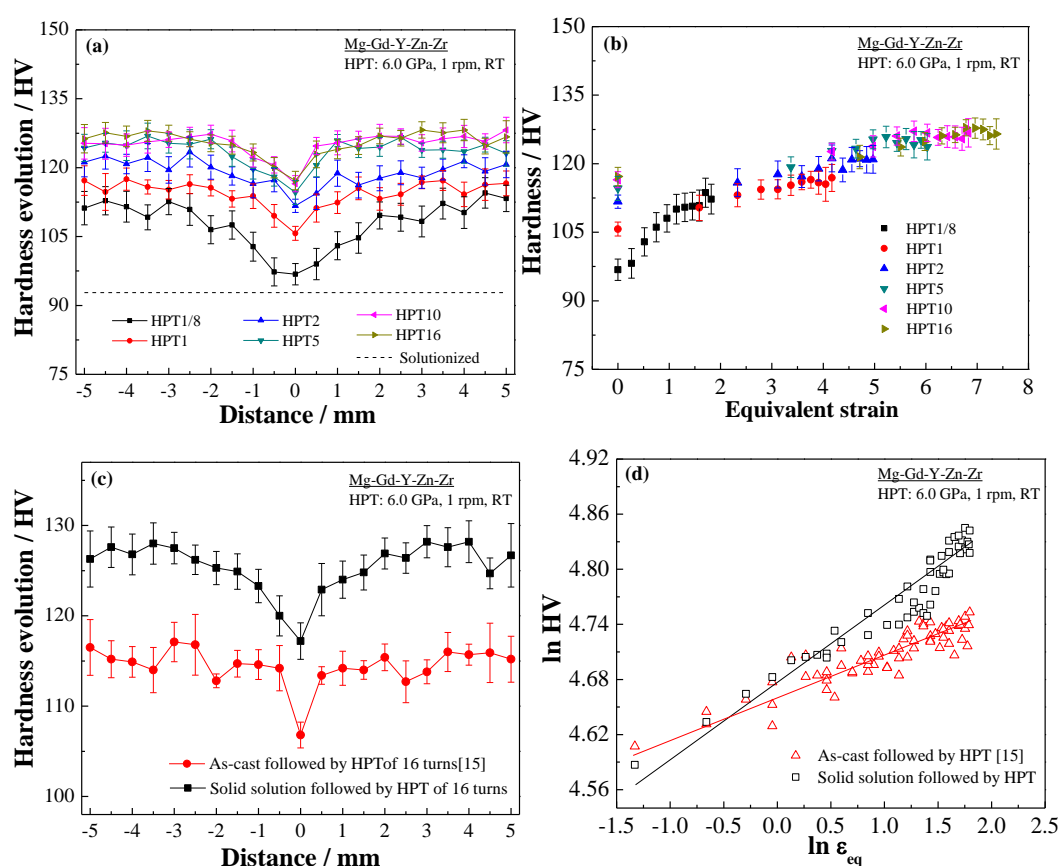


Fig.8 (a) Variation of Vickers microhardness across the diameter of HPT-processed Mg-Gd-Y-Zn-Zr disks with different revolutions (the dashed line indicates the microhardness of initial solutionized alloy); (b) Dependence of Vickers microhardness on the equivalent strain of HPT-processed Mg-Gd-Y-Zn-Zr disks, (c) Comparison of hardness evolution after HPT of 16 turns between as-cast and solid solution, and (d) Double logarithmic plot of microhardness values against equivalent strains up to ~ 6.0 for different initial states followed by HPT processing.

4. Discussions

4.1 Influence of solid solution on microstructure evolution

Our previous research on 16 turns-HPT processing of an as-cast Mg-8.2Gd-3.8Y-1.0Zn-0.4Zr (wt.%) alloy (i.e. with low solute content in the α -Mg phase) [15] has revealed pronounced grain refinement to an average size of $\sim 55 \pm 6$ nm (see the distribution of grain size in Fig. 9), a high dislocation density of $\sim 3.2 \times 10^{14} \text{ m}^{-2}$ and microhardness of $\sim 115 \pm 3$ HV. The present results show that solution treatment prior to HPT causes an even stronger grain refinement and higher dislocation density after HPT deformation resulting in a higher hardness. The mean grain sizes and hardness of pure Mg and a wide range of Mg alloys processed by HPT for different turns at RT as reported in the literatures are summarized in Fig. 10 for comparison [8, 11, 15, 27, 35-44]. Due to the non-uniform hardness distribution from centre to edge in the reported alloys, the values of hardness plotted in Fig. 10 are selected at a representative position with average hardness, the position of half radius of disks. Among these alloys, Mg-RE alloys [8, 11, 37] are subjected to HPT deformation of 5 turns and 10 turns starting from an initial solution-treated condition. During HPT processing the addition of RE elements in Mg alloys causes a more significant refinement than all conventional Mg-rich alloys (see Fig. 10). It can be seen that the present solution-treated and subsequently HPT processed Mg-Gd-Y-Zn-Zr alloy achieves stronger refinement of grains and superior hardness compared to all other Mg-rich alloys.

The higher hardening exponent obtained in the solutionized sample processed by HPT (see Fig. 8(d)) is thought to be due to the more significant increase in dislocation density and more effective grain refinement induced by HPT. In SPD-processed Al alloys some related phenomena have been observed. For example, Morris et al. [45] found that the extent of microstructural refinement and strengthening depended more on solute content than on particle distributions in 6082 Al alloy (Al-Mg-Si) processed by ECAP. A model of grain refinement by Starink et al. [18] included a strong dependency on solute content, and verification by comparison to data on SPD-processed Al alloys confirmed that this solute dependency was seen in a broad range of Al alloys. Also in deformation by cryorolling of a 6063 Al alloy (Al-Mg-Si) the influence of solute content of the Al-rich phase was observed: a stronger work hardening effect was produced for the solution-treated alloy as compared to an aged sample of the same alloy which contained non-coherent and coherent second phase particles [46].

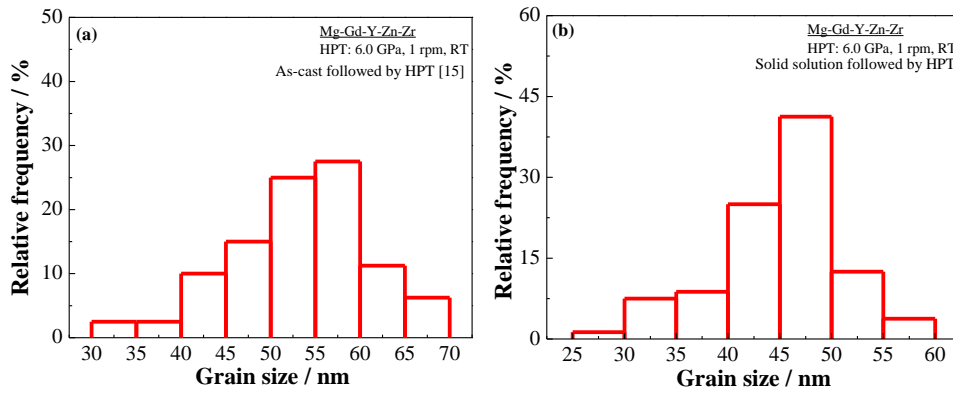


Fig. 9 Histogram for the distribution of grain size: (a) As-cast material processed by HPT [15]; (b) Solid solution treated material processed by HPT.

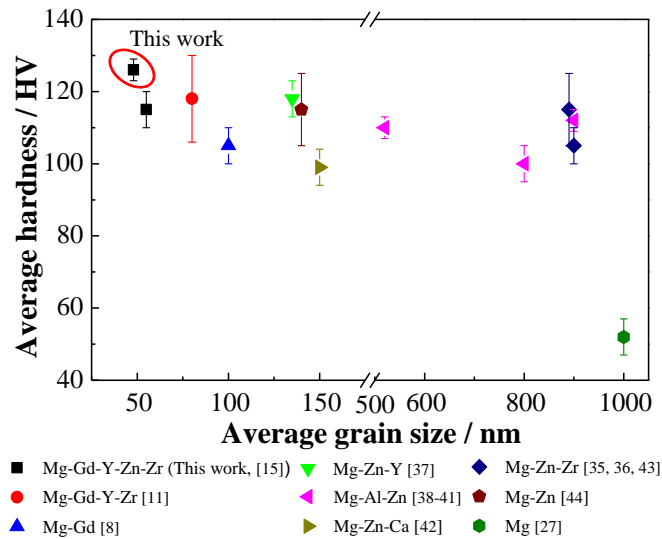


Fig. 10 Comparison of average hardness and grain size in pure Mg and different Mg-rich alloys processed by HPT at room temperature, and the hardness obtained in this work is marked as a red ellipse.

The present results thus reflect that higher dislocation density and enhanced grain refinement of the Mg alloy can be achieved by solution treatment prior to HPT and that the increasing solute atom concentration in the α -Mg is the dominating factor causing this improved efficiency of SPD processing. A possible mechanism is that solutes modify the stacking fault energy (SFE) of the Mg matrix and enhance the pinning effect / solute drag of grain boundaries and dislocations. Experimental data and density functional theory [47-49] indicate that the addition of RE and Zn to Mg matrix significantly reduces the intrinsic SFE, which decreases the probability of cross slipping and climbing for basal dislocations, resulting in reduced dynamic recovery and high dislocation density. Moreover, it is reported that when considering the influence of

dissolved atoms on the dislocation multiplication during SPD, besides geometrically necessary dislocations, the dislocations induced by local bond energies should be taken into account [18]. In other words, when a dislocation passes through the lattice during HPT processing, a pair of solute atoms can be moved to a nearest neighbor constellation that can be energetically unfavourable, and generation of additional dislocations may occur to avoid formation of bonds amongst solute atoms of the same type. As a consequence, a solutionized alloy deformed by HPT should show a more rapid strain hardening than an as-cast counterpart. In addition, these solute atoms are point defects within the α -Mg phase and will enhance the shear stress required for dislocation motion via large solute-matrix mismatch in atomic size, which results in a strong drag from interaction between solutes and dislocations, and thereby the dislocation density may further increase.

EDS results indicate that after HPT the solute elements are dissolved in the matrix, and TEM and XRD analysis illustrate no precipitation has occurred in the grains or along grain boundaries. These are good indications that the supersaturated Mg-rich phase does not decompose during HPT deformation. This is thought to be due to two factors. The present HPT processing temperature is too low to provide thermal energy for diffusion and the generation of intermediate precipitates, either in the matrix or at grain boundaries [50]. The mixing enthalpy of the components in the alloy has a great influence on the decomposition of a solution. For example, the Cu-In supersaturated solid solution with negative mixing enthalpy did not decompose during HPT treatment at RT, and it behaved differently as compared to Cu-Co and Cu-Ni systems with positive mixing enthalpy which promoted the formation of Co-rich and Ni-rich phases respectively [50]. It has even been demonstrated that an Al-Zn supersaturated solid solution with positive mixing enthalpy decomposed to reach a near equilibrium state during HPT at ambient temperature, whereas the decomposition was less pronounced for the Al-Mg alloy with negative mixing enthalpy [51]. It seems that in case of positive mixing enthalpy, HPT processing would speed up the decomposition of supersaturated solid solution by introducing non-equilibrium vacancies [50]. In the present alloy, the Mg, RE, and Zn elements have negative mixing enthalpies for each pair [52-54] as shown in Table 1, which thermodynamically prevents the alloy decomposition during HPT. The solute atoms remaining in the Mg-rich matrix phase may pin the dislocations and impede dislocation movement, retard dislocation annihilation and promote dislocation accumulations in the course of HPT, and therefore influence the ability of non-equilibrium grain boundaries to recover, leading to the very fine grain size observed in the present work.

Table 1 Mixing enthalpy (kJ/mol) between some elements [52, 53, 55-57].

Alloy	Al-Mg	Al-Zn	Cu-In	Co-Cu	Cu-Ni	Mg-Gd	Mg-Y	Mg-Zn
Mixing enthalpy	-2	+1	-5	+10	+11.5	-6	-6	-4

4.2 Correlation between hardening mechanisms and microstructure

The relationship between hardness HV and yield strength σ_y can be approximated by the equation:

$$HV = C\sigma_y \quad (4),$$

where C is a constant about ~ 0.3 , and the units of hardness are taken as HV [58].

To analyse the mechanisms involved in hardening, we will approximate the total Vickers hardness as the combination of grain boundary hardening ΔHV_{GB} , dislocation hardening ΔHV_D and solid solution strengthening ΔHV_{SS} :

$$HV = HV_0 + \Delta HV_{GB} + \Delta HV_D + \Delta HV_{SS} \quad (5),$$

where HV_0 is the microhardness of un-deformed pure Mg, which equals about 6.0 HV [58, 59]. Due to the rather small amount of residual second phase and their relatively large inter-particle spacing, dispersion hardening is very limited and is hence ignored in this analysis. The latter equation should be valid for deformed alloys when further work hardening during indentation in the hardness test is limited.

The effect of grain refinement on hardness increment is usually evaluated by reference to the Hall-Petch equation [20, 58]:

$$\Delta HV_{GB} = Ck_{HP}d^{-1/2} \quad (6),$$

where k_{HP} is the Hall-Petch coefficient, which is reported to be ~ 40.7 MPa / $\mu\text{m}^{-1/2}$ for Mg [58], and d is the mean grain size. For our HPT-processed alloy for which $d=48$ nm this provides $\Delta HV_{GB} = 56$ HV.

The dislocation hardening contribution can be estimated from existing models [58] as follows:

$$\Delta HV_D = CM\alpha_1Gb\sqrt{\rho} \quad (7),$$

where M is the Taylor factor, α_1 is a constant of 0.3, ρ is the dislocation density, G is shear modulus (17.7 GPa for Mg), b is Burgers vector (0.3197 nm for Mg). For our HPT-processed alloy for which the dislocation density is measured to be $4.7 \times 10^{14} \text{ m}^{-2}$ (see Fig. 6) this provides $\Delta HV_D = 28$ HV.

Solid solution strengthening in a ternary or higher order alloy can be approximated using the following relationship [14, 60, 61]:

$$\Delta HV_{SS} = C(\sum k_i^{1/n} c_i)^n \quad (8),$$

where c_i are the concentrations of the corresponding solute atoms. It has been reported that n taken as $1/2$ showed a better description of the yield strength than other values

such as 1, and could satisfactorily predict the ternary solid solution strengthening in Mg-Gd-Y alloys [14]. Therefore, n is set as 1/2 here, and the k_i are factors related to individual solute elements are taken as $683 \text{ MPa(at.\%)}^{-1/2}$, $737 \text{ MPa(at.\%)}^{-1/2}$, $578 \text{ MPa(at.\%)}^{-1/2}$ for Gd, Y and Zn, respectively [14]. EDS data indicated that in the solution treated and subsequently HPT processed samples most of the Gd, Y and Zn present in the alloy was dissolved in the Mg-rich phase, and applying the EDS measured composition of $7.86 \pm 0.02 \text{ wt.\%}$ (equivalent to $\sim 1.3 \text{ at.\%}$) Gd, $3.72 \pm 0.05 \text{ wt.\%}$ (equivalent to $\sim 1.0 \text{ at.\%}$) Y, and $0.65 \pm 0.03 \text{ wt.\%}$ (equivalent to $\sim 0.4 \text{ at.\%}$) Zn provides $\Delta HV_{SS} = 35 \text{ HV}$. In addition, the fairly limited amount of Zr present (0.4 wt.\% , i.e. 0.1 at.\%) assists in grain refinement of magnesium alloys in the course of casting [62], and the Zr is mainly present in second phase particles of typically $1 \mu\text{m}$ in size that have a very high Zr content [16]. Thus the Zr is negligible for solution strengthening and dispersion strengthening.

The sum of the above hardening mechanisms is $\sim 125 \text{ HV}$ which is in excellent agreement with the measured hardness of HPT-processed alloy ($126 \pm 2 \text{ HV}$). It is noteworthy that this means of assessing HV_0 , ΔHV_{GB} and ΔHV_D is consistent with Starink et al. [58] which shows very good model predictions for pure Mg plus many other elements. This illustrates that the hardening factors can be reasonably quantified in the present Mg-Gd-Y-Zn-Zr solid solution with nanosized grains. The above assessment suggests that hardening is mainly determined by grain refinement and stored dislocations whilst solid solution strengthening is responsible for $\sim 28 \%$ of the overall microhardness. In addition to the direct effect through solution strengthening, solute atoms clearly also play an important indirect role through a strong effect on reducing grain size and increasing dislocation density through the solute-dislocation interaction. This can also explain why the microhardness of the present nanostructured solid solution alloy is higher than that of the as-cast samples deformed by HPT [15]. The Mg-Gd-Y-Zn-Zr supersaturated solid solution with nanosized grains and high dislocation density has great potential to be further strengthened by precipitation strengthening through subsequent ageing treatment, which is the object of continuing research.

5. Conclusions

A solution-treated Mg-8.2Gd-3.8Y-1.0Zn-0.4Zr alloy (wt.%) was processed by high pressure torsion (HPT) at room temperature. The conclusions are summarized as follows:

1. With increasing strains imposed by HPT, the microstructure is gradually refined. Following HPT, the dislocation density is increased and the matrix grain size is dramatically reduced to $\sim 48 \text{ nm}$. The residual second phases are further dissolved

in Mg matrix by intense shear straining. Meanwhile, the grain orientation is also changed from initial random texture to basal texture.

2. Comparison with data on processing of an as-cast alloy deformed under the same HPT processing conditions shows that solution treatment before HPT is effective in producing finer grains and a higher dislocation density. The high solute concentration in supersaturated solid solution retards the dislocation annihilation and increases the dislocation density through enhancing the solute-dislocation and / or dislocation-dislocation interactions.
3. The solution-treated Mg-Gd-Y-Zn-Zr alloy exhibits strong strain hardening behavior during HPT and the microhardness reaches ~126 HV at equivalent strain ~6.0. The contribution of each hardening mechanism in nanostructured Mg-Gd-Y-Zn-Zr with supersaturated solid solution is quantitatively evaluated. The overall hardness enhancement is shown to be mainly due to grain boundary hardening and dislocation hardening, with solid solution hardening providing a further contribution. It is reasonable to conclude that improved mechanical properties of Mg alloys can be achieved by proper control of microstructure through heat treatment prior to SPD processing.

Acknowledgement

This work was supported by National Natural Science Foundation of China (No 51571068) and National Key Research and Development Program of China (No. 2016YFB0301102).

References

- [1] B.L. Mordike, T. Ebert, Magnesium: properties-applications-potential, *Mater. Sci. Eng. A* 302 (2001) 37-45.
- [2] M.K. Kulekci, Magnesium and its alloys applications in automotive industry, *Int.J. Adv. Manuf. Technol.* 39 (2008) 851-865.
- [3] A. Luo, M. O. Pekguleryuz, Cast magnesium alloys for elevated temperature applications, *J. Mater. Sci.* 29 (1994) 5259-5271.
- [4] T.L. Chia, M.A. Easton, S.M. Zhu, M.A. Gibson, N. Birbilis, J.F. Nie, The effect of alloy composition on the microstructure and tensile properties of binary Mg-rare earth alloys, *Intermetallics* 17 (2009) 481-490.
- [5] Y.Q. Chi, M.Y. Zheng, C. Xu, Y.Z. Du, X.G. Qiao, K. Wu, X.D. Liu, G.J. Wang, X.Y. Lv, Effect of ageing treatment on the microstructure, texture and mechanical properties of extruded Mg-8.2Gd-3.8Y-1Zn-0.4Zr (wt%) alloy, *Mater. Sci. Eng. A* 565 (2013) 112-117.
- [6] C. Xu, M.Y. Zheng, K.Wu, E.D. Wang, G.H. Fan, S.W. Xu, S. Kamado, X.D. Liu, G.J. Wang, X.Y. Lv, Influence of rolling temperature on the microstructure and mechanical properties of Mg-Gd-Y-Zn-Zr alloy sheets, *Mater. Sci. Eng. A* 559 (2013) 615-622.
- [7] A.P. Zhilyaev, T.G. Langdon, Using high-pressure torsion for metal processing: fundamentals and application, *Prog. Mater. Sci.* 53 (2008) 893-979.
- [8] O. B. Kulyasova, R. K. Islamgaliev, A. R. Kil'mametov, R. Z. Valiev, Superplastic behavior of

- magnesium-based Mg-10 wt % Gd alloy after severe plastic deformation by torsion, *Phys. Met. Metallogr.* 101 (2006) 585-590.
- [9] R. Kocich, L. Kunčická, P. Král, T.C. Lowe, Texture, deformation twinning and hardening in a newly developed Mg-Dy-Al-Zn-Zr alloy processed with high pressure torsion, *Mater. Des.* 90 (2016) 1092-1099.
- [10] L.L. Tang, Y.H. Zhao, N.N. Liang, R.K. Islamgaliev, R.Z. Valiev, Y.T. Zhu, Localized deformation via multiple twinning in a Mg-Gd-Y-Zr alloy processed by high-pressure torsion, *Mater. Sci. Eng. A* 677 (2016) 68-75.
- [11] S.V. Dobatkin, L.L. Rokhlin, E.A. Lukyanova, M.Y. Murashkin, T.V. Dobatkina, N.Y. Tabachkova, Structure and mechanical properties of the Mg-Y-Gd-Zr alloy after high pressure torsion, *Mater. Sci. Eng. A* 667 (2016) 217-223.
- [12] A. Inoue, Y. Kawamura, M. Matsushita, K. Hayashi, J. Koike, Novel hexagonal structure and ultrahigh strength of magnesium solid solution in the Mg-Zn-Y system, *J. Mater. Res.* 16 (2001)1894-1900.
- [13] L. Gao, R.S. Chen, E.H. Han, Solid solution strengthening behaviors in binary Mg-Y single phase alloys, *J. Alloys Compd.* 472 (2009) 234-240.
- [14] L. Gao, R.S. Chen, E.H. Han, Effects of rare-earth elements Gd and Y on the solid solution strengthening of Mg alloys, *J. Alloys Compd.* 481 (2009) 379-384.
- [15] W.T. Sun, C. Xu, X.G. Qiao, M.Y. Zheng, S. Kamado, N. Gao, M.J. Starink, Evolution of microstructure and mechanical properties of an as-cast Mg-8.2Gd-3.8Y-1.0Zn-0.4Zr alloy processed by high pressure torsion, *Mater. Sci. Eng. A* 700 (2017) 312-320.
- [16] C. Xu, M.Y. Zheng, Y.Q. Chi, X.J. Chen, K. Wu, E.D. Wang, G.H. Fan, P. Yang, G.J. Wang, X.Y. Lv, S.W. Xu, S. Kamado, Microstructure and mechanical properties of the Mg-Gd-Y-Zn-Zr alloy fabricated by semi-continuous casting, *Mater. Sci. Eng. A* 549 (2012) 128-135.
- [17] C. Xu, M.Y. Zheng, K. Wu, E.D. Wang, G.H. Fan, S.W. Xu, S. Kamado, X.D. Liu, G.J. Wang, X.Y. Lv, Effect of cooling rate on the microstructure evolution and mechanical properties of homogenized Mg-Gd-Y-Zn-Zr alloy, *Mater. Sci. Eng. A* 559 (2013) 364-370.
- [18] M.J. Starink, X.G. Qiao, J. Zhang, N. Gao, Predicting grain refinement by cold severe plastic deformation in alloys using volume averaged dislocation generation, *Acta Mater.* 57 (2009) 5796-5811.
- [19] A. Thorvaldsen, The intercept method-1. Evaluation of grain shape, *Acta Mater.* 45 (1997) 587-594.
- [20] Y. Chen, N. Gao, G. Sha, S.P. Ringer, M.J. Starink, Microstructural evolution, strengthening and thermal stability of an ultrafine-grained Al-Cu-Mg alloy, *Acta Mater.* 109 (2016) 202-212.
- [21] M. Ferrari, L. Lutterotti, Method for the simultaneous determination of anisotropic residual stresses and texture by X-ray diffraction, *J. Appl. Phys.* 76 (1994) 7246-7255.
- [22] L. Lutterotti, S. Gialanella, X-ray diffraction characterization of heavily deformed metallic specimens, *Acta Mater.* 46 (1998) 101-110.
- [23] G.K. Williamson, R.E. Smallman, Dislocation densities in some annealed and cold-worked metals from measurements on the X-Ray debye-scherrer spectrum, *Philos.Mag.* 1 (1956) 34-46.
- [24] Y.H. Zhao, X.Z. Liao, Z. Jin, R.Z. Valiev, Y.T. Zhu, Microstructures and mechanical properties of ultrafine grained 7075 Al alloy processed by ECAP and their evolutions during annealing, *Acta Mater.* 52 (2004) 4589-4599.
- [25] Pandat software and PanMg database, Release Date: 2017, CompuTherm LLC, Madison, WI, USA, <http://www.computherm.com>.
- [26] I. Saunders, J. Nutting, Deformation of metals to high strains using combination of torsion and compression, *Met. Sci.* 18 (1984) 571-575.
- [27] X.G. Qiao, Y.W. Zhao, W.M. Gan, Y. Chen, M.Y. Zheng, K. Wu, N. Gao, M.J. Starink, Hardening mechanism of commercially pure Mg processed by high pressure torsion at room

- temperature, *Mater. Sci. Eng. A* 619 (2014) 95-106.
- [28] M.L. Fornasini, P. Manfrinetti, GdMg₅: a complex structure with a large cubic cell, *Acta Crystallogr. C* 42 (1986) 138-141.
- [29] Y. Estrin, A. Molotnikov, C.H.J. Davies, R. Lapovok, Strain gradient plasticity modelling of high-pressure torsion, *J. Mech. Phys. Solids* 56 (2008) 1186-1202.
- [30] J. Crump, X.G. Qiao, M.J. Starink, The effect of high-pressure torsion on the behaviour of intermetallic particles present in Al-1Mg and Al-3Mg, *J. Mater. Sci.* 47 (2012) 1751-1757.
- [31] J. Peng, L.P. Zhong, Y.J. Wang, Y. Lu, F.S. Pan, Effect of extrusion temperature on the microstructure and thermal conductivity of Mg-2.0Zn-1.0Mn-0.2Ce alloys, *Mater. Des.* 87 (2015) 914-919.
- [32] Q.M. Peng, J. Meng, Y.D. Li, Y.D. Huang, N. Hort, Effect of yttrium addition on lattice parameter, Young's modulus and vacancy of magnesium, *Mater. Sci. Eng. A* 528 (2011) 2106-2109.
- [33] H.L. Ding, X.B. Shi, Y.Q. Wang, G.P. Cheng, S. Kamado, Texture weakening and ductility variation of Mg-2Zn alloy with CA or RE addition, *Mater. Sci. Eng. A* 645 (2015) 196-204.
- [34] F. Yang, T.W. Fan, J. Wu, B.Y. Tang, L.M. Peng, W.J. Ding, Effects of Y and Zn atoms on the elastic properties of Mg solid solution from first-principles calculations, *Phys. Status Solidi B* 248 (2011) 2809-2815.
- [35] H.J. Lee, S.K. Lee, K.H. Jung, G.A. Lee, B. Ahn, M. Kawasaki, T.G. Langdon, Evolution in hardness and texture of a ZK60A magnesium alloy processed by high-pressure torsion, *Mater. Sci. Eng. A* 630 (2015) 90-98.
- [36] H.J. Lee, B. Ahn, M. Kawasaki, T.G. Langdon, Evolution in hardness and microstructure of ZK60A magnesium alloy processed by high-pressure torsion, *J. Mater. Res. Technol.* 4 (2015) 18-25.
- [37] A. Singh, D.A. Basha, H. Somekawa, K. Tsuchiya, Nucleation of recrystallized magnesium grains over quasicrystalline phase during severe plastic deformation of a Mg-Zn-Y alloy at room temperature, *Scr. Mater.* 134 (2017) 80-84.
- [38] L.R.C. Malheiros, R.B. Figueiredo, T.G. Langdon, Grain size and microhardness evolution during annealing of a magnesium alloy processed by high-pressure torsion, *J. Mater. Res. Technol.* 4 (2015) 14-17.
- [39] Y. Huang, R.B. Figueiredo, T. Baudin, A.L. Helbert, F. Brisset, T.G. Langdon, Effect of temperature on the processing of a magnesium alloy by high-pressure torsion, *J. Mater. Sci.* 47 (2012) 7796-7806.
- [40] Y. Huang, R.B. Figueiredo, T. Baudin, F. Brisset, T.G. Langdon, Evolution of strength and homogeneity in a magnesium AZ31 alloy processed by high-pressure torsion at different temperatures, *Adv. Eng. Mater.* 14 (2012) 1018-1026.
- [41] M. Kai, Z. Horita, T.G. Langdon, Developing grain refinement and superplasticity in a magnesium alloy processed by high-pressure torsion, *Mater. Sci. Eng. A* 488 (2008) 117-124.
- [42] O.B. Kulyasova, R.K. Islamgaliev, Y.H. Zhao, R.Z. Valiev, Enhancement of the mechanical properties of an Mg-Zn-Ca alloy using high-pressure torsion, *Adv. Eng. Mater.* 17 (2015) 1738-1741.
- [43] S.A. Torbati-Sarraf, T.G. Langdon, Properties of a ZK60 magnesium alloy processed by high-pressure torsion, *J. Alloy. Compd.* 613 (2014) 357-363.
- [44] F.Q. Meng, J.M. Rosalie, A. Singh, H. Somekawa, K. Tsuchiya, Ultrafine grain formation in Mg-Zn alloy by in situ precipitation during high-pressure torsion, *Scr. Mater.* 78-79 (2014) 57-60.
- [45] I.G. Urrutia, M. Morris, D.G. Morris, The effect of coarse second-phase particles and fine precipitates on microstructure refinement and mechanical properties of severely deformed Al alloy, *Mater. Sci. Eng. A* 394 (2005) 399-410.

- [46] S.K. Panigrahi, R. Jayaganthan, Influence of solutes and second phase particles on work hardening behavior of Al 6063 alloy processed by cryorolling, *Mater. Sci. Eng. A* 528 (2011) 3147-3160.
- [47] B. Smola, I. Stulikova, J. Pelcova, B.L. Mordike, Significance of stable and metastable phases in high temperature creep resistant magnesium-rare earth base alloys, *J. Alloys Compd.* 378 (2004) 196-201.
- [48] M. Suzuki, T. Kimura, J. Koike, K. Maruyama, Effects of zinc on creep strength and deformation substructures in Mg-Y alloy, *Mater. Sci. Eng. A* 387-389 (2004) 706-709.
- [49] S. Sandlöbes, M. Friák, S. Zaeferrer, A. Dick, S. Yi, D. Letzig, Z. Pei, L.F. Zhu, J. Neugebauer, D. Raabe, The relation between ductility and stacking fault energies in Mg and Mg-Y alloys, *Acta Mater.* 60 (2012) 3011-3021.
- [50] B.B. Straumal, A.R. Kilmametov, A.A. Mazilkin, L. Kurmanaeva, Y. Ivanisenko, A. Korneva, P. Zięba, B. Baretzky, Transformations of Cu(in) supersaturated solid solutions under high-pressure torsion, *Mater. Lett.* 138 (2015) 255-258.
- [51] B.B. Straumal, B. Baretzky, A.A. Mazilkin, F. Phillipp, O.A. Kogtenkova, M.N. Volkov, R.Z. Valiev, Formation of nanograined structure and decomposition of supersaturated solid solution during high pressure torsion of Al-Zn and Al-Mg alloys, *Acta Mater.* 52 (2004) 4469-4478.
- [52] A. Takeuchi, A. Inoue, Calculations of mixing enthalpy and mismatch entropy for ternary amorphous alloys, *Mater. Trans.* 41 (2000) 1372-1378.
- [53] A. Takeuchi, A. Inoue, Classification of bulk metallic glasses by atomic size difference, heat of mixing and period of constituent elements and its application to characterization of the main alloying element, *Mater. Trans.* 46 (2005) 2817-2829.
- [54] W.J. Ding, Y.J. Wu, L.M. Peng, X.Q. Zeng, G.Y. Yuan, D.L. Lin, Formation of 14H-type long period stacking ordered structure in the as-cast and solid solution treated Mg-Gd-Zn-Zr alloys, *J. Mater. Res.* 24 (2009) 1842-1854.
- [55] S. Knott, A. Mikula, Calorimetric investigation of the binary Cu-In system, *Int. J. Mater. Res.* 97 (2006) 1098-1101.
- [56] C. Gente, M. Oehring, R. Bormann, Formation of thermodynamically unstable solid solutions in the Cu-Co system by mechanical alloying, *Phys. Rev. B Condensed Matter*, 48 (1993) 13244-13252.
- [57] H.W. Yang, D.P. Tao, Z.H. Zhou, Prediction of the mixing enthalpies of binary liquid alloys by molecular interaction volume model, *Acta Metall. Sin-Engl. Lett.* 21 (2008) 336-340.
- [58] M.J. Starink, X. Cheng, S. Yang, Hardening of pure metals by high-pressure torsion: A physically based model employing volume-averaged defect evolutions, *Acta Mater.* 61 (2013) 183-192.
- [59] G.V. Samsonov (Ed.), *Handbook of the physicochemical properties of the elements* (2nd ed.), Plenum Press, New York (1968).
- [60] L.A. Gypen, A. Deruyttere, Multi-component solid solution hardening, *J. Mater. Sci.* 12 (1977) 1028-1033.
- [61] Z. Zhu, M.J. Starink, Solution strengthening and age hardening capability of Al-Mg-Mn alloys with small additions of Cu, *Mater. Sci. Eng. A* 488 (2008) 125-133.
- [62] M. Qian, A. Das, Grain refinement of magnesium alloy by zirconium: Formation of equiaxed grains, *Scr. Mater.* 54 (2006) 881-886.